Nanotoxicology, 2011; Early Online, 1–14

Cd/Se/Te-based quantum dot 705 modulated redox homeostasis with hepatotoxicity in mice

CHIA-HUA LIN[1], MO-HSIUNG YANG[2,3], LOUIS W. CHANG[1], CHUNG-SHI YANG[3], HAN CHANG[4], WAN-HSUAN CHANG[1], MING-HSIEN TSAI[1], CHIEN-JEN WANG[1], & PINPIN LIN[1]

[1]*Division of Environmental Health and Occupational Medicine, National Health Research Institutes, Zhunan,* [2]*Department of Biomedical Engineering and Environmental Sciences, National Tsing Hua University, Hsinchu,* [3]*Center for Nanomedicine Research, National Health Research Institutes, Zhunan, and* [4]*Department of Pathology, China Medical University Hospital, Taichung, Taiwan*

(Received 8 July 2010; accepted 9 November 2010)

Abstract

The objective of this study was to investigate whether quantum dot 705 (QD705) disrupts the cellular antioxidant systems leading to hepatotoxicity in mice. Mice were intravenously injected with QD705 and then sacrificed at week 12 or 16. Homeostasis of antioxidant-related metals, antioxidant activities, induction of oxidative stress, and toxicity in the liver were investigated. Although no histopathological change was observed, a time- and dose-dependent increase in metallothionein expression and reduction in liver function was noticed. Increased copper, zinc, and selenium levels and enhancements of the trace metal-corresponding transporters were noted at week 12. At week 16, a decline of selenium from its elevated level at week 12 was observed, which was accompanied by changes in glutathione peroxidase activity as well as in redox status. A significant reduction in superoxide dismutase activity was observed at 16 weeks. Furthermore, a corresponding elevation of heme oxygenase-1 expression, 8-oxo-7,8-dihydro-2′-deoxyguanosine, interleukin-6 and tumor necrosis factor-alpha suggested the presence of oxidative stress, oxidative DNA damage and inflammation.

Keywords: *Nanoparticles, QD705, cadmium, mice, oxidative DNA damage, hepatotoxicity*

Introduction

Quantum dots (QDs) are inorganic nanocrystals with a unique autofluorescent property with great potential for diagnosis and drug delivery (Gao et al. 2004; Mulder et al. 2010; Obonyo et al. 2010). They also have applications as semiconductors in the electronics industry (Haridas and Basu 2010; Wu et al. 2004). Typical QDs are 2–10 nm in diameter, with a metalloid crystalline core surrounded by a thin shell or cap (Dabbousi et al. 1997; Deng et al. 2010). Coating the QD surface with a mono- or multi-layer of molecules can prevent agglomeration and reduce core metal leaching (Hardman 2006). Additional surface coating can also be applied for specific applications, such as increasing the fluorescent efficiency, solubility in biological media, or bio-conjugation to antibodies for specific diagnostic and therapeutic purposes (Gao et al. 2004; Mulder et al. 2010). QD705, our test material, is a cadmium/selenium/tellurium (CdSeTe)-based nanocrystal (Invitrogen, Inc.) which emits stable near-infrared fluorescence and thus has promising potential for medical imaging applications (Gao et al. 2008; Smith et al. 2008).

Despite the exciting potential and growing interest in biological applications of QDs, concerns remain regarding the potential accumulation and toxic effects of QDs in animals and humans (Hoshino et al. 2004b; Zhang et al. 2008; Das et al. 2010).

Several *in vitro* studies on QD-induced toxic potentials have been reported but the conclusions were controversial (Jaiswal et al. 2003; Shiohara et al. 2004; Hoshino et al. 2004a; Lovric et al. 2005; Chan and Shiao 2008; Monteiro-Riviere et al. 2009; Mahto et al. 2010). Most toxic assessments of QDs were conducted under *in vitro* conditions

Correspondence: Dr Pinpin Lin, National Health Research Institutes, Environmental Health & Occupational Medicine, Zhunan, Taiwan. Tel: +886 37 246 166 ext. 36508. Fax: +886 37 587 406. E-mail: pplin@nhri.org.tw

ISSN 1743-5390 print/ISSN 1743-5404 online © 2011 Informa UK, Ltd.
DOI: 10.3109/17435390.2010.539712

and far fewer *in vivo* studies were performed (Geys et al. 2008; King-Heiden et al. 2009; Hauck et al. 2010). More recently, Hauck et al. (2010) reported that intravenous injection of QDs failed to change tissue morphology, parameters of clinical biochemistry or hematology in rats 80 days later. However, these parameters were relatively insensitive for chronic toxicities. More *in vivo* mechanistic-based toxicology studies are needed to assess the safety of QDs.

Our previous studies demonstrated extremely long body retention of QD705 in mice after intravenous injection and liver appeared to be one of the target organs of QD705 accumulation (Yang et al. 2007; Lin et al. 2008). We also found that biodegradation of QD705 can occur *in vivo* with leakage or release of Cd to the cells (Lin et al. 2009). Indeed, there are studies which suggested that the QD-induced toxic mechanism may be related to the presence of free Cd^{2+} and the formation of reactive oxygen species (ROS) (Cho et al. 2007). Most of the *in vitro* studies suggested that the bases of QD toxicity, if any, are probably related to oxidative stress (Chan et al. 2006; Choi et al. 2007; Lee et al. 2009; Clift et al. 2010). Cellular redox homeostasis may therefore play an important role in QD-induced cytotoxicity.

Cellular redox status is primarily controlled by antioxidant systems, including the glutathione (GSH) and glutathione peroxidase (GPx) system and the antioxidant enzymes such as superoxide dismutase (SOD) and catalase (CAT). These antioxidant systems help to safeguard the balance of ROS level within biological systems. A reduction in functions of such antioxidant systems would certainly lead to elevated levels of ROS. Functions of these antioxidant systems are closely influenced by levels of intracellular essential trace metals, such as copper (Cu), zinc (Zn), iron (Fe), manganese (Mn), and Se (Endo et al. 2000; Hasegawa et al. 2008).

Cd, a non-essential metal, has been reported to compete with many essential trace metals, including Fe, Mn, Cu, and Zn, and disrupt the activities of metal transporter molecules on cell membranes (He et al. 2006; Min et al. 2008). Such disruption would alter antioxidant functions. This study examined the interrelationship of QD705 exposure with disturbance of antioxidant systems (trace metal homeostasis, antioxidant enzyme activities, etc.) and eventual oxidative stress.

Although Cd-based QDs induced cytotoxicity and oxidative stress *in vitro* studies (Cho et al. 2007; Choi et al. 2007; Lee et al. 2009; Clift et al. 2010), another study demonstrated that injection of CdSe-based QDs was not toxic within 80 days in rats (Hauck et al. 2010). In the present study, we examined the effects of QD705 on redox homeostasis in the liver of mice up to 16 weeks (112 days) after injection. The information generated may provide insight into the mechanisms of the toxicity risk of QDs in biological systems.

Materials and methods

Test chemicals

The QD705 nanoparticles used in our experiments were purchased from Invitrogen, Inc. (Hayward, CA, USA) as Qtracker 705 non-targeted quantum dots. QD705 contained the Cd/Se/Te core covered with a ZnS shell and modified with methoxy-PEG-5000 coating. Each tube of this product contained 200 μL of 2 μM solution in 50 mM borate buffer, pH 8.3.

Animal studies

Six-week-old male ICR mice were purchased from BioLASCO (Taiwan) and acclimated for two weeks in the animal facilities at the National Health Research Institutes (NHRI). All animal treatments and experimental protocols for this study were reviewed and approved by the Animal Control Committee at NHRI. Mice were maintained under a 12-h light/dark cycle, 23 ± 1°C, 39–43% relative humidity, with water and food available *ad libitum*. Six mice (n = 6) per time point were randomly selected for experimentation. Mice were injected via tail veins with 40 and 160 pmol of QD705 in borate buffer with volume of 100 μL/mouse. The intravenous (iv) administration route was chosen to mimic potential human medical imaging applications. Mice were sacrificed under pentobarbital anesthesia at 12 and 16 weeks after dosing. The liver was carefully removed, weighed, and prepared for metal analyses and other studies.

Physicochemical characterization of QD705

QD705 were characterized for size distribution, zeta potential, size, and shape. The hydrodynamic diameters and zeta potentials of QD705 were measured with the Zetasizer Nano system (Zetasizer Nano ZS, Malvern Instruments, Worcestershire, UK). Dynamic laser light scattering measurements were checked in the single-scattering regime with λ = 633 nm and at an angle of 173°. QD705 were suspended in borate buffer and sonicated up to 60 min. The suspension was put into a cuvette at 25°C to enable particle size and zeta potential analysis. The shape and size of QD705 were assessed by transmission electron

microscopy (TEM) (H-7650, Hitachi, Japan). QD705 were suspended in borate buffer. The QD705 solution was then dripped on copper grids for TEM. All of the copper grids were preserved in a dry cabinet. The fluorescence and absorbance spectra were measured using a fluorescence spectrometer (Cary Eclipse, Varian, USA).

Histopathology and tissue preparation

Tissue specimens from the livers were fixed in buffered 10% formalin for 48 h prior to tissue processing (dehydration and paraffin embedding). Sections were cut at 3 μm thick with rotary microtome. Hematoxylin and eosin (H&E) were used for general histology staining in accordance to standard H&E staining procedures.

Immunohistostaining method

Metallothionein-1/2 (MT) immunohistochemistry has been described as previous study (Lin et al. 2009). Briefly, heating 10 min in autoclave for antigen retrieval was essential. The anti-MT was a specific antibody for metallothionein-1/2 and used in 1:100 dilution. By following, a standard immunostaining assay was performed as the reagent instructions (LSAB, DakoCytomation, Carpinteria, CA, USA). The slides were further stained with hematoxylin.

Quantification of serum alanine aminotransferase (ALT) and aspartate aminotransferase (AST) activity

Serum was isolated from the blood of experimental mice and then stored at −80°C until analysis. Serum ALT and AST activities were analyzed using a Vitros 350 autoanalyzer (Ortho-Clinical Diagnostics, Johnson & Johnson Co., NJ, USA) with accompanying commercial kits.

Quantitative real-time reverse transcription–polymerase chain reaction (RT–PCR) assay

Tissues (n = 6) soaked in RNA later solution were incubated at 4°C overnight and then transferred to −80°C until RNA purification. Tissues were ground with a tissue homogenizer (MM301, Retsch Technology GmbH, Haan, Germany) in TRIZOL reagent (Life Technologies, Rockville, MD, USA), and then total RNA was purified via chloroform extraction. Purified RNA was stored at −80°C until analysis. cDNA was synthesized using the High-Capacity cDNA Archive kit (P/N4322171, Applied Biosystems, Foster City, CA, USA) with total RNA (3 μg). The primers sequences for Zrt- and irt-related protein (ZIP) 8, ZIP14, copper transporter 1 (CTR-1) are listed in Table I. Quantitative PCR for ZIP8, ZIP14, and CTR-1 was performed using SYBR Green PCR system (Applied Biosystems, Foster City, CA, USA). The reaction mixture was prepared by mixing aliquots of cDNA, 0.4 μM primers and 5 μl of SYBR Green PCR Master Mix (Applied Biosystems, Foster City, CA, USA) in a final volume of 10 μL. The primers and probe for heme oxygenase-1 (HO-1), tumor necrosis factor-alpha (TNF-α), interleukin-1 beta (IL-1β), interleukin-6 (IL-6), chemokine (C-X-C motif) ligand 1 (CXCL1) and glyceraldehyde-3-phosphate dehydrogenase (GAPDH) were included in the Assay-on-Demand Gene Expression Assay Mix (Applied Biosystems, Foster City, CA, USA) (Table I). Quantitative PCR for HO-1, TNF-α, IL-1β, IL-6 and CXCL1 was performed using TaqMan Universal PCR Master Mix (Applied Biosystems, Foster City, CA, USA). The reaction mixture was prepared by mixing aliquots of cDNA,

Table I. The gene accession code, assay ID and primer sequences.

Gene symbol	Gene name	Accession code	Assay ID or sequences
GAPDH	glyceraldehyde-3-phosphate dehydrogenase	NM_008084	Mm99999915_g1
HO-1	heme oxygenase 1	NM_010442	Mm00516004_m1
CXCL1	chemokine (C-X-C motif) ligand 1	NM_008176	Mm00433859_m1
IL-6	interleukin 6	NM_031168	Mm00446191_m1
IL-1β	interleukin 1 beta	NM_008361	Mm00434228_m1
TNF-α	tumor necrosis factor alpha	NM_013693	Mm00443258_m1
CTR-1	Cu transporter-1	NM_175090	F: 5′-GCCTTCGTGGCAGTGTTTTT-3′ R: 5′-GCGAATGCTGACTTGAGACTTTC-3′
ZIP8	zrt- and Irt-related protein 8	NM_026228	F: 5′-GCAACAATTTTGCTCCCAAT-3′ R: 5′-TCCCTATGGAGATGTTTCTGTG-3′
ZIP14	zrt- and Irt-related protein 14	NM_144808	F: 5′-CATTGAAGTATGGGGGTACGGT-3′ R: 5′-ATGAAGTAGAGCAGGAGCCTCT-3′

0.5 μL of Assay-on-Demand Gene Expression Assay Mix and 5 μL of TaqMan Universal PCR Master Mix (Applied Biosystems, Foster City, CA, USA) in a final volume of 10 μL. The reaction mixture was analysed on an ABI PRISM 7900 Sequence Detector System (Applied Biosystems, Foster City, CA, USA) with the following PCR program: 95°C for 10 min followed by 40 cycles of 60°C for 1 min with 95°C for 15 sec.

Quantitative values were obtained from the threshold cycle (Ct) number. The relative mRNA levels of target gene were derived using the equation $2^{-\Delta Ct}$, where $\Delta Ct = Ct_{\ target\ gene} - Ct_{GAPDH}$. Data are presented as the fold of the control value.

Inductively coupled plasma mass spectrometry (ICP-MS) assay

ICP-MS (Elan6100; PerkinElmer, Shelton, CT, USA) was used to determine the Cu, Mn, Se, and Zn, and Fe concentrations in the liver. Briefly, partial organs ($n = 6$) were dried with a lyophilizer at −50°C for 24 h, then weighed (approximately 30 mg) and liquefied with 0.5 mL nitric acid and subjected to microwave digestion (Multiwave 3000; Anton Paar GmbH, Graz, Austria). The microwave digestion temperature was programmed to increase from 30–75°C at a rate of 7.5°C/min with a 1 min hold at 75°C and up to 130°C at a rate of 11°C/min with a hold of 30 min at 130°C (Anton Paar GmbH, Graz, Austria). The digested solution (0.5 mL) was diluted to 10 mL with 3.5% HNO_3 in deionized water. This sample solution was then directly analyzed for ^{111}Cd, ^{65}Cu, ^{55}Mn, ^{82}Se, and ^{66}Zn, and ^{57}Fe. Standard solutions, 0.1, 0.5, 1, 5, 10, 50, 100, and 500 $\mu g \cdot L^{-1}$ (Cu, Mn, Se, and Zn, and Fe in 3.5% HNO_3), were used for sample quantification. The efficiency of digestion procedures was tested using the certified reference material, European Commission CRM 185R, Trace Element in Lyophilized Bovine Liver (the certified values for Cu, Mn, Se, and Zn are 277 ± 5, 110.7 ± 0.29, 1.68 ± 0.14, and 138.6 ± 2.1 mg/kg, while no data was available for Fe). The obtained recoveries for Cu, Mn, Se, and Zn of 89, 93, 92, and 93% ($n = 3$). The method detection limits for Cu, Mn, Se, and Zn, and Fe were 0.066, 0.090, 0.24, 7.2, and 4.9 $\mu g \cdot L^{-1}$, respectively. All steps in sample preparation and measurements were carried out in a chemical hood.

Measurement of reduced glutathione (GSH)/glutathione disulfide (GSSG) ratio

Tissues were rinsed with phosphate buffered saline (PBS) and then ground with a tissue homogenizer (MM301, Retsch Technology GmbH, Haan, Germany) in cold buffer (50 mM MES, pH 6–7, containing 1 mM EDTA). The liver homogenates were centrifuged at 10,000 *g* for 15 min at 4°C. The supernatants were deproteinated and then collected for analysis of GSH and GSSG according to the manufacturer's protocol (Cayman Chemical Company, Ann Arbor, MI, USA). Visible absorbance was recorded at 405 nm using an ELISA plate reader.

Measurement of GPx activity

Tissues were rinsed with PBS and then ground with a tissue homogenizer (MM301, Retsch Technology GmbH, Haan, Germany) in cold buffer (50 mM Tris-HCl, pH 7.5, containing 5 mM EDTA, and 1 mM DTT). The liver homogenates were centrifuged at 10,000 *g* for 15 min at 4°C. The supernatants were collected for analysis of GPx according to the manufacturer's protocol (Cayman Chemical Company, Ann Arbor, MI, USA). Visible absorbance was recorded at 340 nm using an ELISA plate reader.

Measurement of Cu/Zn- and Mn-SOD activity

Tissues were rinsed with PBS and then ground with a tissue homogenizer (MM301, Retsch Technology GmbH, Haan, Germany) in cold buffer (20 mM HEPES buffer, pH 7.2, containing 1 mM EGTA, 210 mM mannitol, and 70 mM sucrose). The liver homogenates were centrifuged at 1,500 *g* for 5 min at 4°C. The supernatants were collected for analysis of Cu/Zn- and Mn-SOD according to the manufacturer's protocol (Cayman Chemical Company, Ann Arbor, MI, USA). Visible absorbance was recorded at 450 nm using an ELISA plate reader.

Quantification of 8-oxo-7,8-dihydro-2′-deoxyguanosine (8-oxodG)

DNA was isolated from liver tissue according to the method of Ravanat et al. (2002) with modifications. DNA was then spiked with $[^{15}N_5]$-8-oxodG and $[^{15}N_5]$-dG for quantitation of 8-oxodG and dG by online SPE LC-MS/MS using a polyamine-II endcapped HPLC column (150 × 2 mm, 5 μm, YMC) at a flow rate of 300 $\mu L min^{-1}$. The analytes eluted from the HPLC system were then introduced into a triple-quadrupole mass spectrometer (API 3000, Applied Biosystems/MDS SCIEX, concord, Ontario, Canada), operating with a TurbolonSpray source (Chao et al. 2008).

Statistical analysis

Comparison of the results between various experimentally treated groups and their corresponding controls was carried out by Student's *t*-test. All comparisons were considered significantly different when $p < 0.05$.

Results

Physicochemical Properties of QD705

The particle shape and size of QD705 were characterized by TEM. As shown in Figure 1A, the QD705 were spherical-shaped nanoparticles with sizes of about 12.3 ± 5.2 nm. The averaged particle size of QF705 in borate buffer was 143.3 nm and the size distribution was between 10 nm and 250 nm (Figure 1B). The 152.7 nm peak was aggregated QD705. As shown in Table II, the zeta potential of QD705 in borate buffer was −24.8 ± 5.1 mV. Aggregates of QD705 were insoluble and remained dispersed in borate buffer for at least 1 h. The maximal emission of QD705 was about 705 nm (λ_{ex} = 350 nm) (Figure 1C).

Histopathology and MT immunohistochemistry of liver in QD705-treated mice

Regardless of the doses or time post-treatment, the histology of mouse livers showed no remarkable change by the H&E stain (Figure 2A). In control mouse livers, MT protein was detected in some hepatocytes around the portal areas (zone 1) (Figure 2B).

The distribution and intensity of MT immunostaining in QD705-treated mouse livers was dose-dependent, but similar at 12 and 16 weeks. In 40 pmol QD705-treated mice livers, MT protein showed a distinct zonal distribution. While MT-positivity occurred mainly in zone 1 hepatocytes and zone 2 hepatocytes, the hepatocytes around the

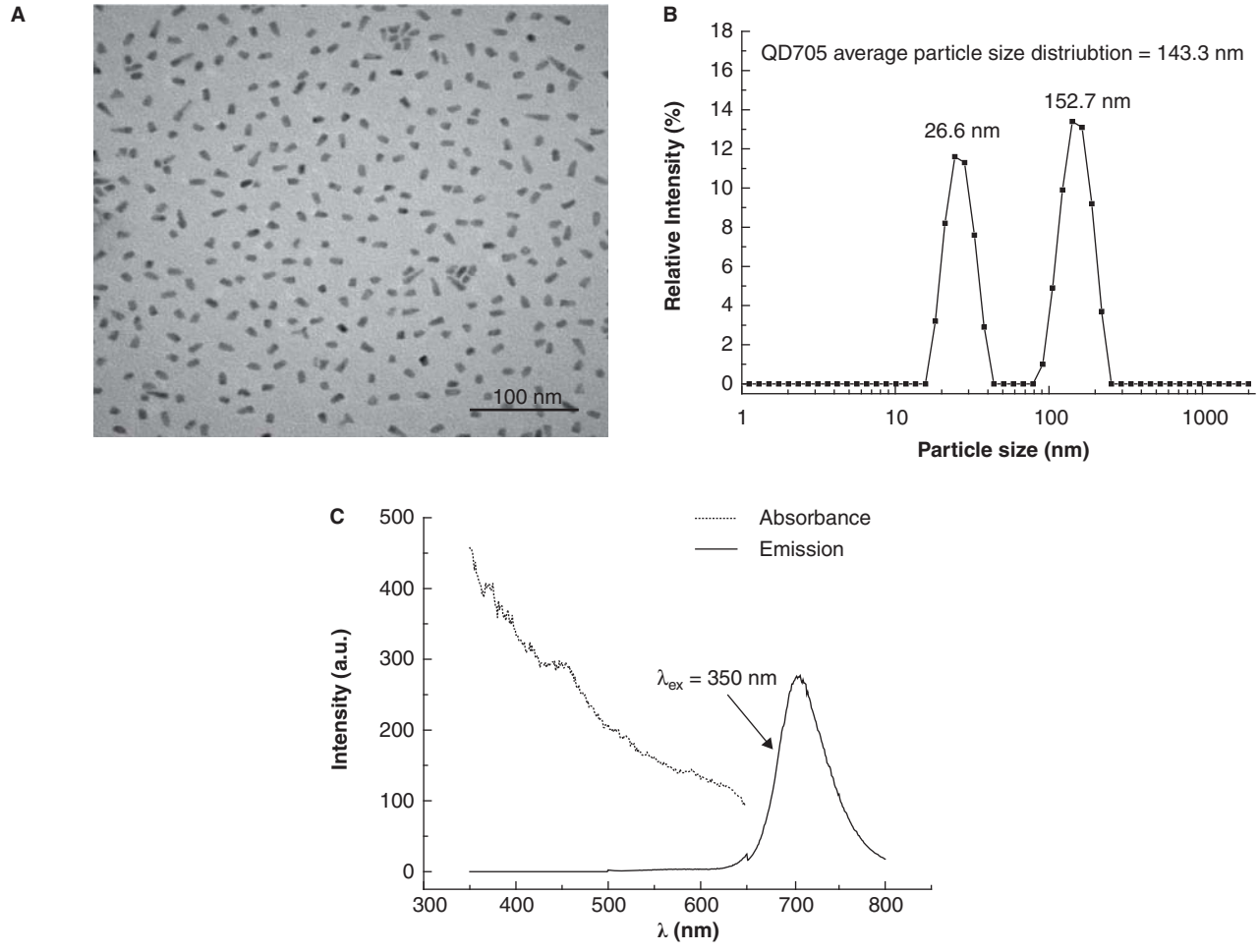

Figure 1. Physicochemical properties of QD705. (A) TEM micrograph of the QD705 nanoparticles. (B) Particle size distribution of QD705 in borate buffer. (C) The absorption and emission spectra of the QD705: the maximal emission at about 705 nm for excitation at 350 nm.

Table II. Physicochemical properties of QD705.

Parameter	Characterization
Form	Suspension (suspended in borate buffer)
Composition	Cd(56.16 ± 8.54%) / Se(5.80 ± 3.60%) / Te(0.92 ± 0.20%), ZnS, PEG5000
Shape	The core/shell of QD705 is ellipsoid in shape. After application of the polymer, PEG, the QD705 become more spherical.
Particle size/distribution	In dry form, the size is 12.3 ± 5.2 nm (TEM); in borate buffer, the size is 143.3 nm (DLS).
Solubility/dispersibility	Aggregates are insoluble and remain dispersed in borate buffer.
Zeta potentials	−24.8 ± 5.1 mV

central vein areas (zone 3) were almost all MT-negative or -weakly positive (Figure 2C). MT staining intensity was more intense in 160 pmol than 40 pmol QD705-treated mouse livers. Furthermore, the zonal distribution of MT protein was not obvious in 160 pmol QD705-treated mouse livers, but the zone 1 hepatocytes still showed more intense MT staining than zone 3 hepatocytes (Figure 2D).

QD705 induced injury in the liver

Liver injury was assessed by measuring serum activities of ALT and AST. At 12 weeks post-injection, a significant elevation in ALT activity was observed at high dose (160 pmol) (Figure 3A). This elevation remained significant at 16 weeks and a similar elevation was found in mice-treated with low dose (40 pmol) of QD705 (Figure 3A). While no significant change was observed in AST activity at 12 weeks, a significant elevation in AST activity was detected at 16 weeks in mice treated with the high dose (160 pmol) of QD705 (Figure 3B).

QD705 induced changes of essential trace metals in the liver

Oxidative stress may be closely related to dysfunction of the antioxidation systems: SOD, CAT, and the glutathione system. All of these major antioxidation systems require specific trace metals for their activities: Cu, Zn for cytosol SOD, Mn for mitochondrial SOD, Fe for CAT, and Se for the glutathione system. The present study revealed that QD705 provided interesting alterations in these trace metals. By the 12th week of QD705 treatment, the most noticeable change was an increase in Cu, Zn,

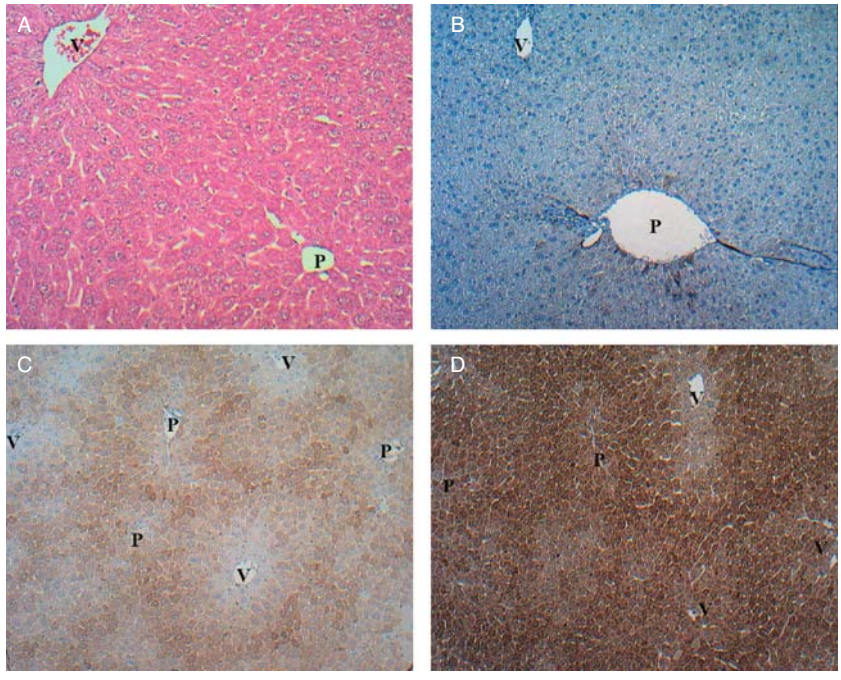

Figure 2. Histopathology and MT immunohistochemistry of liver in QD705-treated mice sacrificed at 12th week. (A) H&E staining for 40 pmol QD705-treated mice (×200). (B) MT IHC for the liver of control mice (×200). MT occasionally expressed in zone 1 hepatocytes (×200). (C) MT IHC for the liver of 40 pmol QD705-treated mice (×100). MT expressed as a zonal distribution. (D) MT IHC for the liver of 160 pmol QD705-treated mice (×100). MT diffusely expressed in hepatic lobules. P represents as portal area and V represents as central vein in figures.

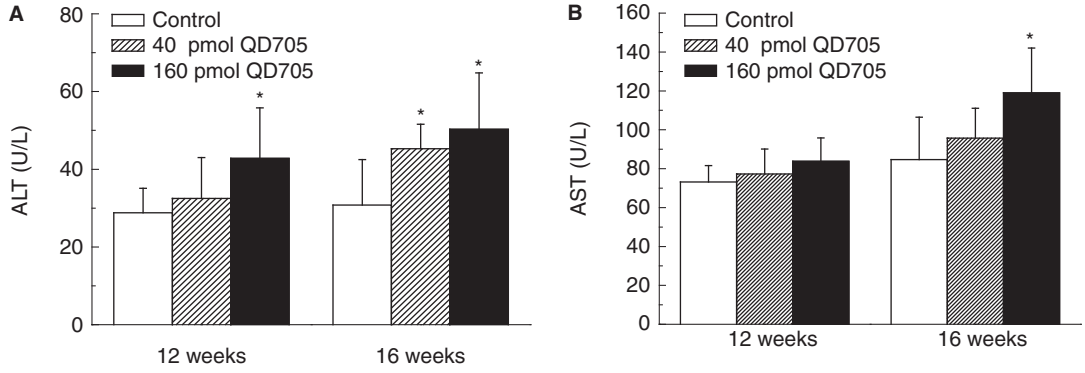

Figure 3. Change in hepatic enzyme activities in serum by QD705 (A) ALT. A significant elevation of ALT was observed at high dose (160 pmol) at 12 weeks. This elevation remained significant at 16 weeks. (B) AST. A significant elevation of AST activity was detected at 16 weeks. *indicates $p < 0.05$ as compared with vehicle-treated mice.

and Se in the liver as compared to those levels in controls (Table III). By the 16th week of QD705 treatment, however, the Cu level had returned to normal, and Zn and Se levels were reduced somewhat but still slightly higher than normal (Table III). The most noticeable change at the 16th week was the significant reduction of Mn in the liver (Table III).

QD705 induced expression of essential trace metal transporter genes in the liver

We assessed whether QD705 treatment affects the expression of trace metal transporters, including, ZIP8 (a known Mn transporter), ZIP14 (a known Zn transporter) and CTR-1 (a known Cu transporter). At 12 weeks after injection, ZIP14 and CTR-1 mRNA levels were significantly elevated, whereas ZIP8 mRNA level was not significantly changed (Figure 4). At later times after exposure (16 weeks), however, when the mRNA levels of ZIP14 and CTR-1 had returned to normal, while ZIP8 mRNA level was elevated (Figure 4).

QD705 induced antioxidant enzymes activity in the liver

We examined three antioxidant systems in the liver: GPx, Cu, Zn-SOD, and Mn-SOD. After injection of QD705, a significant elevation of GPx activity was observed at 12 weeks (Figure 5A). This elevation remained significant at 16 weeks even at a higher dose (160 pmol); however, the GPx activities had declined at 16 weeks from the highly elevated levels at 12 weeks (Figure 5A). While no significant change was observed in Cu or Zn-SOD activity at 12 weeks, a significant reduction of Cu/Zn-SOD activity was

Table III. Effects of QD705 on essential trace metal concentrations (μg/g wet wt.) in liver at 12 and 16 weeks after tail vein injection and Cd to ICR mice.

Time after exposure (weeks)	Metals	Control ($n = 6$) (μg/g wet wt.)	QD705 40 pmol ($n = 6$) (μg/g wet wt.)	QD705 160 pmol ($n = 6$) (μg/g wet wt.)
12	Mn	1.08 ± 0.26	1.23 ± 0.21	1.37 ± 0.24
	Cu	4.53 ± 0.73	6.04 ± 1.46*	6.70 ± 0.82*
	Zn	31.66 ± 4.10	37.72 ± 3.63*	51.68 ± 15.75*
	Se	1.71 ± 0.17	2.06 ± 0.27*	3.05 ± 0.29*
	Fe	217.95 ± 28.35	250.35 ± 66.15	211.74 ± 61.15
16	Mn	1.33 ± 0.11	1.10 ± 0.08*	1.14 ± 0.11*
	Cu	6.05 ± 1.11	6.38 ± 1.40	7.21 ± 2.05
	Zn	31.87 ± 2.35	36.29 ± 4.71*	35.66 ± 2.71*
	Se	2.10 ± 0.11	1.99 ± 0.12	2.77 ± 0.19*
	Fe	217.34 ± 44.80	261.30 ± 73.38	241.21 ± 46.07

ICR mice were injected with QD705. Sacrifices were carried out at 12 and 16 weeks after dosing. The liver was isolated to determine essential trace metal concentrations with ICP-MS. The data are the mean ± SD of six animals. * indicates a significant difference from control ($p < 0.05$).

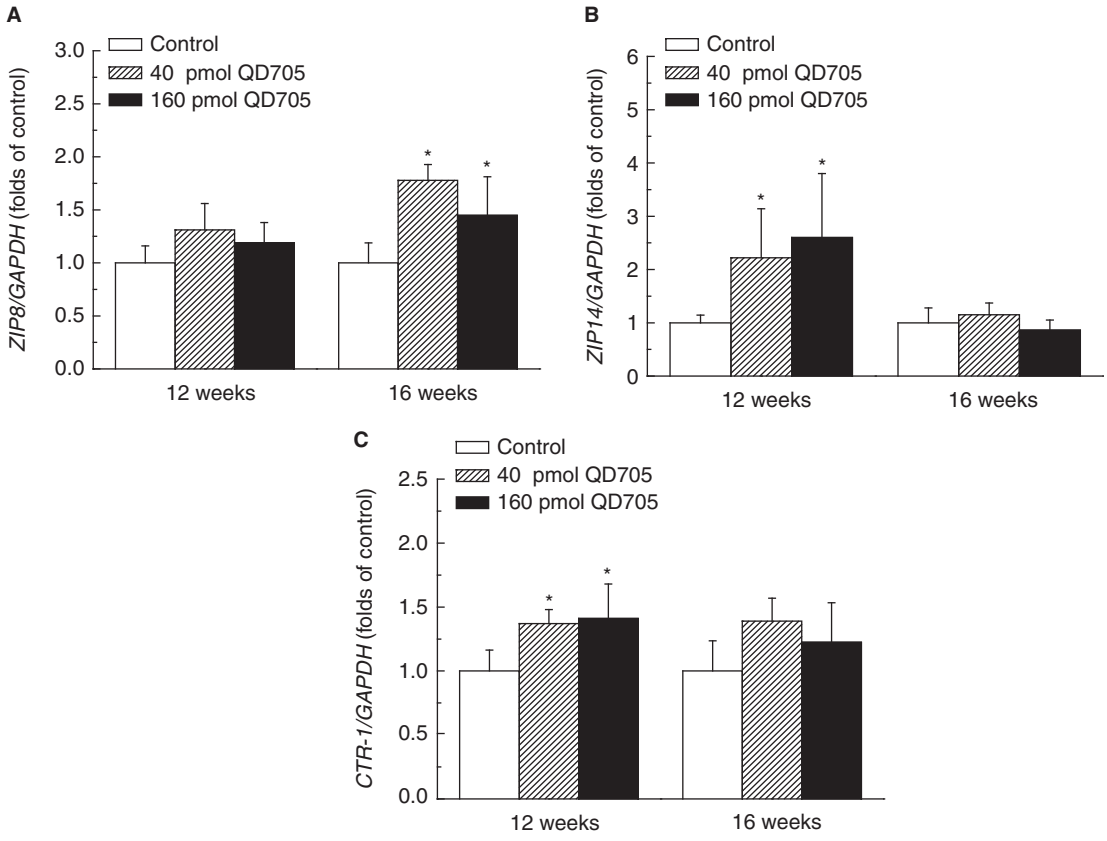

Figure 4. Change in metal transporters expression in the liver by QD705. (A) ZIP8: Mn transporter. Significant elevations of ZIP8 were observed at 16 weeks after QD705 exposure. (B) ZIP14: Zn transporter. Although significant stimulatory elevations were observed at 12 weeks after QD705 exposure, such elevations were temporary and the ZIP14 returned to normal level by 16 weeks. (C) CTR-1: mRNA gene expression of Cu transporter. As in ZIP14, temporary elevations were observed under QD705 exposure at 12 weeks but subsided by 16 weeks. *indicates $p < 0.05$ as compared with vehicle-treated control cells.

detected at 16 weeks in liver of animals treated with the higher dose (160 pmol) of QD705 (Figure 5B). No significant change in Mn-SOD was found in the liver of QD705-treated animals compared with controls (Figure 5C).

QD705 induced oxidative stress responses in the liver

The ratio of GSH/GSSG is frequently used as a sensitive index of oxidative status in biological systems (Griffith 1999). A reduction in the ratio of GSH/GSSG is reflective of oxidative stress. In this study, at 12 weeks, the GSH/GSSG ratio was significantly elevated in all animals exposed to QD705 (Figure 6A). However, this ratio was significantly reduced by 16 weeks in QD705-treated animals compared with controls (Figure 6A).

HO-1 is considered an indicator of oxidative stress and 8-oxo-dG is a biomarker for ROS-induced genotoxicity in biological systems (Griffith 1999; Danielsen et al. 2008). Although there were no significant changes in these two oxidative indicators at 12 weeks, there were dose-correlated elevations on both HO-1 and 8-oxo-dG in the liver of QD705-treated animals at 16 weeks (Figure 6B, 6C).

MT-1 gene is inducible by various metallic elements, especially in the liver and kidney. Cd is a potent inducer of MT-1. QD705 induced significant elevation in hepatic MT-1 mRNA levels at 12 weeks post-exposure (Figure 6D). MT-1 induction persisted through 16 weeks (Figure 6D).

QD705 induced pro-inflammatory factors in the liver

Pro-inflammatory cytokines are usually activated in response to oxidative stress (Hehlgans and Pfeffer 2005; Han et al. 2009). Dose-correlated elevations in TNF-α and IL-6 mRNA levels were detected in the livers of QD705-treated mice at 16 weeks (Figures 7A, 7C). However, no significant change in IL-1β and CXCL1 mRNA levels was observed (Figure 7B, 7D).

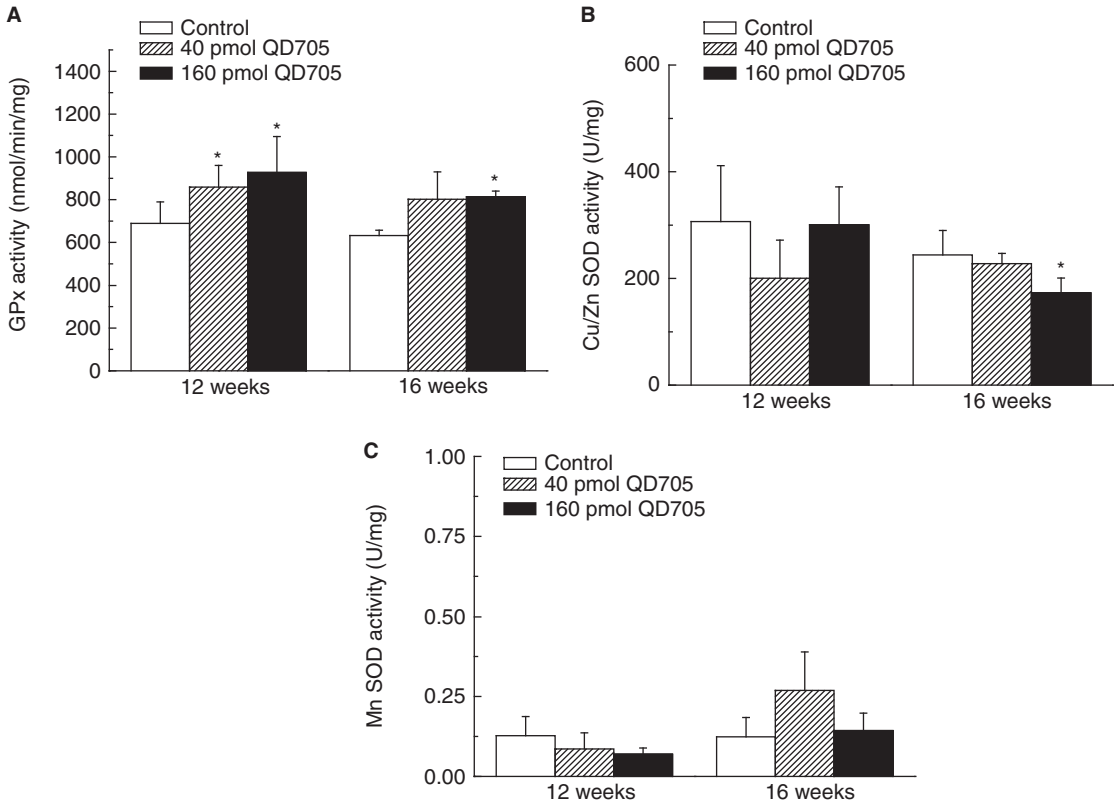

Figure 5. Change in antioxidant enzymes activity in the liver by QD705 (A) GPx. A significant elevation of GPx was observed at 12 weeks but rapidly declined by 16 weeks. (B) Cu/Zn-SOD. Except at high dose (160 pmol) and for long term (16 weeks) exposure, there was a reduction of SOD level and no significant change in Cu/Zn-SOD level was observed. (C)Mn-SOD. No change was observed in Mn-SOD activity. *indicates $p < 0.05$ as compared with vehicle-treated mice.

Discussion

Most previous studies on QD-induced ROS were conducted *in vitro* and their results may not actually reflect *in vivo* responses. Recently Hauck et al. (2010) demonstrated that intravenous injection of CdSe-based QDs failed to cause appreciable toxicity in rats over a period of 80 days. In the present study, we demonstrated CdTeSe-based QD705-induced adverse responses in mouse liver up to 12 weeks post-injection. The doses (pmol/body weight) used in our present study were slightly lower than those used in Hauck's study. The different results of these two studies may be explained by the differences in metal components of QDs or animal species. Indeed, Cho et al. (2007) reported that CdSe-based QDs were non-toxic, whereas the CdTe-based QDs were cytotoxic *in vitro*. It implied that Te may involve in the cytotoxicity induced by CdTe-based QDs. Generation of ROS is believed to be the basis for QD-induced toxicity (Samia et al. 2003; Ipe et al. 2005; Lovric et al. 2005; Cho et al. 2007).

This *in vivo* study demonstrated three important phenomena:

(1) Time-related changes of trace metal transporters (ZIP8, ZIP14, and CTR-1) and trace metals (Se, Cu, Zn, Mn) which are important for the integrity of antioxidation systems;
(2) Dose-correlated reduction of antioxidative status (GSH/GSSG ratio) by QD705; and
(3) Corresponding elevations of oxidative stress markers (HO-1 and 8-oxo-dG), the pro-inflammatory cytokines (TNF-α and IL-6) and liver injury markers (ALT and AST).

In some established models for chemical-induced hepatotoxicity, ALT and AST activities were tremendously elevated within days (Lores Arnaiz et al. 1995; Moreno and Muriel 2006; Honda et al. 2010). In our present study, QD705 treatment only significantly elevated ALT activity to approximately 30% of controls at week 12. Compared to other studies, the doses of QD705 (pmol/g body weight) used in our present study were much lower than those of typical hepatotoxicants (μmol/g body weight) used in other studies (Lores Arnaiz et al. 1995; Moreno and Muriel 2006; Honda et al. 2010). Because our QD705 doses

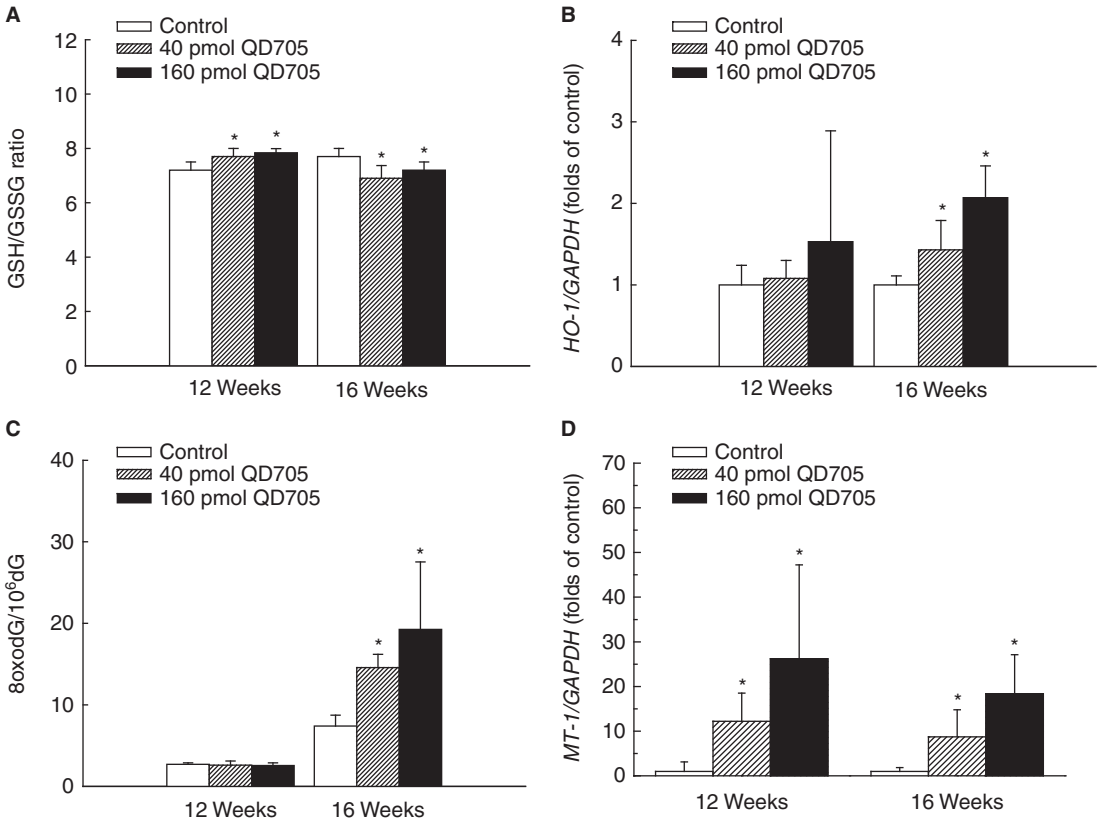

Figure 6. Change in redox status, oxidative stress markers, and cellular injury factor. (A) GSH/GSSG ratio (index for redox status). A biphasic change in the redox status was observed: A stimulataneous increase at 12 weeks and a significant reduction at 16 weeks were noted. (B) HO-1 expression. HO-1, a recognized factor reflecting oxidative stress, was significantly elevated by QD705 at 16 weeks after exposure. (C) 8-oxo-dG (factor indicative of oxidative DNA damage). Similar to HO-1, this factor was also significantly elevated at 16 weeks. (D) MT-1 expression. QD705 induced significant elevation in MT-1 mRNA levels in the liver at 12 and 16 weeks. * indicates $p < 0.05$ as compared with vehicle-treated mice.

were similar to those used for animal imaging studies (Gao et al. 2004; Cai et al. 2006), our data shall be appropriate for assessing QD705 safety in clinical application.

The major anti-oxidative systems in cells are the SOD, catalase, and glutathione systems. Of these, the glutathione (GSH/GSSG) and the SOD systems are the most important (Sies 1993). The activity of SOD is closely affiliated with the homeostasis of Cu and Zn (Cu/Zn-SOD) in cytosol and with Mn (Mn-SOD) in mitochondria (Endo et al. 2000; Hasegawa et al. 2008). The present study found stimultaneous increases of both Cu and Zn and slight enhancements of the transporters for Cu and Zn (CTR-1 and ZIP14, respectively) in the liver of QD-treated mice. These enhancements are thought to be compensatory in nature. That is, upon challenge by QD705 or Cd^{2+} release, a compensatory increase of Cu and Zn may be induced during the early exposure period as an attempt to maintain the anti-oxidation potential of Cu/Zn-SOD in the liver. A decompensatory response was observed at a later time (16 weeks) after QD705 exposure with significant reduction in Cu/Zn-SOD activity.

ZIP 8 and ZIP14 are ZIP family members. It has been suggested that ZIP8 transported Zn, Mn, and Cd, and ZIP14 transported Zn, Mn, Cd, and Fe (Himeno et al. 2009). Recently, Besecker et al. (2008) demonstrated that TNF-α can up-regulate ZIP8 expression. In our present study, consistent with the elevation of TNF-α, ZIP8 mRNA levels were increased at week 16. On the other hand, ZIP14 expression was modulated by IL-1β via activator protein-1 involved pathways (Lichten et al. 2009). Human CTR-1 plays an important role in maintenance of copper homeostasis (Song et al. 2008). Increased CTR-1 expression and function lead to increased intracellular copper content (Song et al. 2008). Indeed, both CTR-1 mRNA and Cu levels were transiently elevated at week 12 in our present study. Sp-1 transcription factor functioned as a sensor of copper that regulated CTR-1 mRNA levels (Song et al. 2008). Both ZIP14 and CTR-1 mRNA levels was transiently

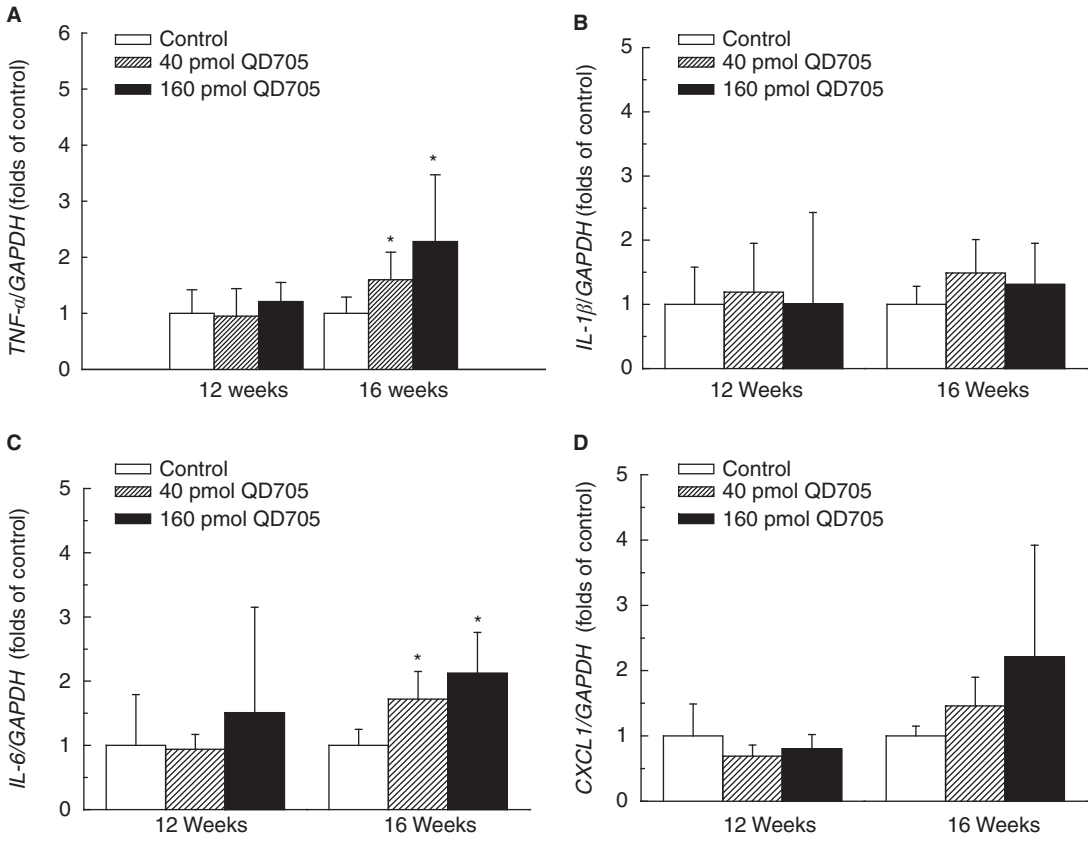

Figure 7. Change in pro-inflammatory factors. (A) TNF-α expression. TNF-α (a pro-inflammatory factor indicative an early cell injury), was significantly elevated at 16 weeks after QD705 exposure. (B) IL-1β expression. No change was observed. (C) IL-6 expression. Similar to TNF-α, IL-6 was also significantly elevated at 16 weeks. (D) CXCL1 expression. No significant change was observed. *indicates $p < 0.05$ as compared with vehicle-treated mice.

elevated at 12 weeks. However, the mechanism was still unclear.

The glutathione system, however, showed a different response to challenge with QD705. A significant increase in Se, which is a cofactor of GPx, was observed in the liver of animals at 12 weeks of QD705 exposure. This surge of Se level in the liver coincided well with the increase of GPx activity in the liver at this time. A slight decline of Se was noted at 16 weeks which was also coincidental with a reduction of GPx activity in the liver. This change in the glutathione system denotes a 'two-stage' event of QD-induced cellular response: An initial compensatory stage with an increase of GPx activity upon QD challenge and an eventual decompensatory stage with an actual reduction of GPx. Similarly, anti-oxidation status (GSH/GSSG) ratio also fitted 'two-stage' event: An enhancement of GSH/GSSG ratio at compensatory stage (12 weeks) with the declination at a later time (16 weeks). Total glutathione was also elevated at 12 weeks and the absolute levels of GSH were declined over time (data not shown). It appears that the liver tried to increase anti-oxidation capabililty at compensatory stage (12 weeks). Once the anti-oxidation system could not completely remove QD705-induced oxidative stress, the liver entered the decompensatory stage with reduced anti-oxidation capability (reduced GSH/GSSG) and more adverse responses.

The question remains whether this decrease in anti-oxidation status after QD705 exposure would actually lead to oxidative stress. Cellular oxidative stress and oxidative damage to DNA may be indicated by the elevations of two factors: HO-1 and 8-oxo-dG (Danielsen et al. 2008). Furthermore, inflammation may also be reflected by the enhancement of the pro-inflammatory factor, TNF-α (Hehlgans and Pfeffer 2005). Indeed, the present study demonstrated significant elevations in all of these factors (HO-1, 8-oxo-dG, TNF-α, ZIP8, ALT, and AST) in a dose-correlated fashion at the late stage of exposure (16 weeks). Thus, this study has demonstrated, for the first time, that injection of QD705 into animals (mice) suppresses anti-oxidation status (glutathione system) in the liver and causes oxidative stress, and hepatotoxicity.

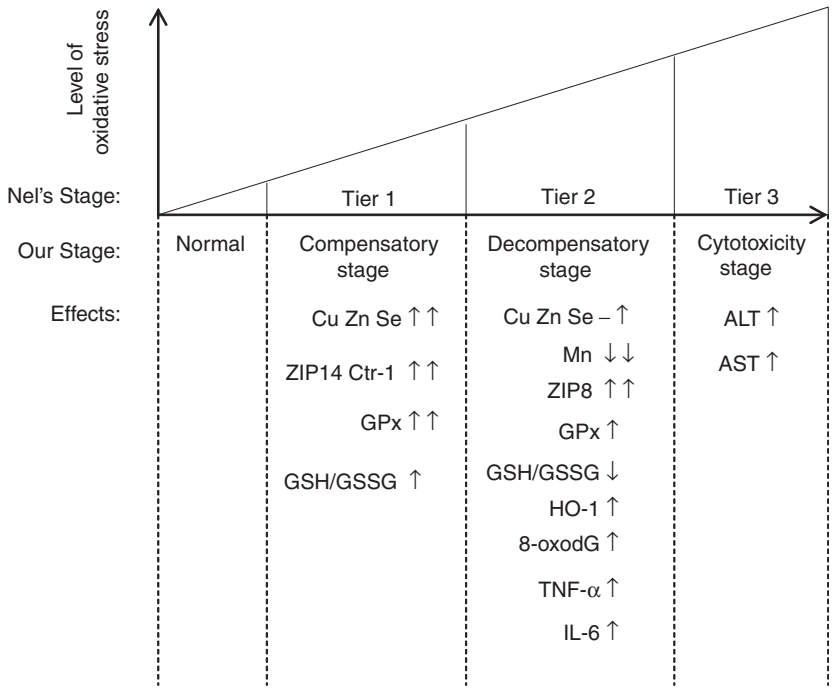

Figure 8. Model of hierarchical oxidative stress and response induced by QD705 in the liver of ICR mice. The various events (changes in trace metals, redox status, oxidative stress index, etc.) induced by QD705 in the liver of mice are summarized.

Nel et al. (2006) recently proposed that the oxidative stress induced by nano-materials may occur in a three-tiered sequence. Tier 1 of the sequence is the initial response to the challenge with cellular anti-oxidation defense; Tier 2 is failing of the defense system with overwhelming ROS accumulation accompanied by induction of oxidative stress and inflammation; and Tier 3 is cytotoxicity with mitochondrial damage, cellular injury, and apoptosis. The findings in the present study are consistent with this 3-Tier Model (Figure 8). By 12 weeks, a compensatory response was found in the liver with enhanced levels of trace elements (Se, Cu, and Zn) which are important for maintaining the integrity of anti-oxidation systems such as the glutathione (GPx), Cu, and Zn-SOD. This compensatory response appears to be equivalent to Tier 1 of the model proposed by Nel et al. (2006). At a later time (16 weeks) after exposure to QD705, we found a reduction of GSH/GSSG ratio (anti-oxidation status) with elevation of oxidative stress markers (HO-1 and 8-oxo-dG), TNF-α and ZIP8 in the liver. These findings support the hypothesis of a decompensatory stage represented by Tier 2 of the model of Nel et al. (2006). A significant increase in ALT and AST was observed in the liver of QD705-treated mice at 16 weeks. This result reveals that with longer experimental time, cytotoxic change (liver injury) can also be induced by QD705 (Tier 3 of the Nel Model).

However, a significant elevation of ALT was also observed at high dose (160 pmol) of QD705 at 12 weeks. It suggests that more mechanisms may contribute to hepatotoxicity induced by the high dose of QD705. It seems that only our results at low dose (40 pmol) were consistent with the Nel's model. Most studies evaluated the safety of nanomaterials by assessing their cytotoxicity and inflammatory effects. Genotoxicity is one of the major criteria for assessing health risk of new pharmaceuticals and clinically used chemicals (Singh et al. 2009).

Genotoxicity not only could initiate or promote tumorgenesis, but also has adverse effects on fertility. However, genotoxicity of nanomaterials are rarely investigated (Singh et al. 2009). In our present study, QD705 caused the formation of 8-oxo-dG in mice liver. If 8-oxo-dG is not removed by 8-oxogaunine-DNA glycosylase-1 (OGG1), a DNA repair enzyme, during cell proliferation this DNA adduct can lead to DNA mutation. Cadmium ion has been demonstrated to inhibit OGG1 expression and activity (Zharkov and Rosenquist 2002; Youn et al. 2005). Previously, we reported that QD705 might decompose and release cadmium ion *in vivo* (Lin et al. 2009).

Therefore, the combined effects of cadmium ion and 8-oxodG formation would greatly enhance the mutation risk following QD705 treatment. Data from this study support the hypothesis that the oxidative-related responses induced by QD705 are

closely related to the free Cd released from these nanocrystals (Cho et al. 2007). However, it should be noted that both intact QD705 and free Cd are present in the liver even after 16 weeks of exposure (Lin et al. 2009). The result of the present study certainly cannot exclude the possibility of direct toxic impacts by intact QD705 in QD705-treated mice.

Declaration of interest: This work was supported by grant NM-097-PP08 and NM-098-PP08 from the Center for Nanomedicine Research, National Health Research Institutes, Zhunan, Taiwan. The authors report no conflict of interest. The authors alone are responsible for the content and writing of the paper.

References

Besecker B, Bao S, Bohacova B, Papp A, Sadee W, Knoell DL. 2008. The human zinc transporter SLC39A8 (Zip8) is critical in zinc-mediated cytoprotection in lung epithelia. Am J Physiol Lung Cell Mol Physiol 294:L1127–1136.

Cai W, Shin DW, Chen K, Gheysens O, Cao Q, Wang SX, et al. 2006. Peptide-labeled near-infrared quantum dots for imaging tumor vasculature in living subjects. Nano Lett 6:669–676.

Chan WH, Shiao NH. 2008. Cytotoxic effect of CdSe quantum dots on mouse embryonic development. Acta Pharmacol Sin 29:259–266.

Chan WH, Shiao NH, Lu PZ. 2006. CdSe quantum dots induce apoptosis in human neuroblastoma cells via mitochondrial-dependent pathways and inhibition of survival signals. Toxicol Lett 167:191–200.

Chao MR, Yen CC, Hu CW. 2008. Prevention of artifactual oxidation in determination of cellular 8-oxo-7,8-dihydro-2′-deoxyguanosine by isotope-dilution LC-MS/MS with automated solid-phase extraction. Free Radic Biol Med 44:464–473.

Cho SJ, Maysinger D, Jain M, Roder B, Hackbarth S, Winnik FM. 2007. Long-term exposure to CdTe quantum dots causes functional impairments in live cells. Langmuir 23:1974–1980.

Choi AO, Cho SJ, Desbarats J, Lovric J, Maysinger D. 2007. Quantum dot-induced cell death involves Fas upregulation and lipid peroxidation in human neuroblastoma cells. J Nanobiotechnol 5:1.

Clift MJ, Boyles MS, Brown DM, Stone V. 2010. An investigation into the potential for different surface-coated quantum dots to cause oxidative stress and affect macrophage cell signalling in vitro. Nanotoxicology 4:139–149.

Dabbousi BO, Rodriguez-Viejo J, Mikulec FV, Heine JR, Mattoussi H, Ober R, et al. 1997. (CdSe)ZnS core-shell quantum dots: Synthesis and characterization of a size series of highly luminescent nanocrystallites. J Phys Chem 101:9463–9475.

Danielsen PH, Risom L, Wallin H, Autrup H, Vogel U, Loft S, et al. 2008. DNA damage in rats after a single oral exposure to diesel exhaust particles. Mutat Res 637:49–55.

Das GK, Chan PPY, Teo A, Loo JSC, Anderson JM, Tan TTY. 2010. In vitro cytotoxicity evaluation of biomedical nanoparticles and their extracts. J Biomed Materials Res A 93A:337–346.

Deng Z, Schulz O, Lin S, Ding B, Liu X, Wei X, et al. 2010. Aqueous synthesis of zinc blende CdTe/CdS magic-core/thick-shell tetrahedral-shaped nanocrystals with emission tunable to near-infrared. J Am Chem Soc 132:5592–5593.

Endo T, Fujii T, Sato K, Taniguchi N, Fujii J. 2000. A pivotal role of Zn-binding residues in the function of the copper chaperone for SOD1. BiochemBiophys Res Communic 276: 999–1004.

Gao X, Cui Y, Levenson RM, Chung LW, Nie S. 2004. In vivo cancer targeting and imaging with semiconductor quantum dots. Nat Biotechnol 22:969–976.

Gao X, Wang T, Wu B, Chen J, Yue Y, Dai N, et al. 2008. Quantum dots for tracking cellular transport of lectin-functionalized nanoparticles. Biochem Biophys Res Commun 377: 35–40.

Geys J, Nemmar A, Verbeken E, Smolders E, Ratoi M, Hoylaerts MF, et al. 2008. Acute toxicity and prothrombotic effects of quantum dots: Impact of surface charge. Environ Health Perspect 116:1607–1613.

Griffith OW. 1999. Biologic and pharmacologic regulation of mammalian glutathione synthesis. Free Radic Biol Med 27:922–935.

Han D, Ybanez MD, Ahmadi S, Yeh K, Kaplowitz N. 2009. Redox regulation of tumor necrosis factor signaling. Antioxid Redox Signal 11:2245–2263.

Hardman R. 2006. A toxicologic review of quantum dots: Toxicity depends on physicochemical and environmental factors. Environ Health Perspect 114:165–172.

Haridas M, Basu JK. 2010. Controlled photoluminescence from self-assembled semiconductor-metal quantum dot hybrid array films. Nanotechnology 21:415202.

Hasegawa S, Koshikawa M, Takahashi I, Hachiya M, Furukawa T, Akashi M, et al. 2008. Alterations in manganese, copper, and zinc contents, and intracellular status of the metal-containing superoxide dismutase in human mesothelioma cells. J Trace Elem Med Biol 22:248–255.

Hauck TS, Anderson RE, Fischer HC, Newbigging S, Chan WC. 2010. In vivo quantum-dot toxicity assessment. Small 6:138–144.

He L, Girijashanker K, Dalton TP, Reed J, Li H, Soleimani M, et al. 2006. ZIP8, member of the solute-carrier-39 (SLC39) metal-transporter family: Characterization of transporter properties. Mol Pharmacol 70:171–180.

Hehlgans T, Pfeffer K. 2005. The intriguing biology of the tumour necrosis factor/tumour necrosis factor receptor superfamily: Players, rules and the games. Immunology 115:1–20.

Himeno S, Yanagiya T, Fujishiro H. 2009. The role of zinc transporters in cadmium and manganese transport in mammalian cells. Biochimie 91:1218–1222.

Honda A, Komuro H, Hasegawa T, Seko Y, Shimada A, Nagase H, et al. 2010. Resistance of metallothionein-III null mice to cadmium-induced acute hepatotoxicity. J Toxicol Sci 35:209–215.

Hoshino A, Fujioka K, Oku T, Suga M, Sasaki YF, Ohta T, et al. 2004a. Physicochemical properties and cellular toxicity of nanocrystal quantum dots depend on their surface modification. Nano Letters 4:2163–2169.

Hoshino A, Hanaki K, Suzuki K, Yamamoto K. 2004b. Applications of T-lymphoma labeled with fluorescent quantum dots to cell tracing markers in mouse body. Biochem Biophys Res Commun 314:46–53.

Ipe BI, Lehnig M, Niemeyer CM. 2005. On the generation of free radical species from quantum dots. Small 1:706–709.

Jaiswal JK, Mattoussi H, Mauro JM, Simon SM. 2003. Long-term multiple color imaging of live cells using quantum dot bioconjugates. Nat Biotech 21:47–51.

King-Heiden TC, Wiecinski PN, Mangham AN, Metz KM, Nesbit D, Pedersen JA, et al. 2009. Quantum dot nanotoxicity assessment using the zebrafish embryo. Environ Sci Technol 43:1605–1611.

Lee HM, Shin DM, Song HM, Yuk JM, Lee ZW, Lee SH, et al. 2009. Nanoparticles up-regulate tumor necrosis factor-alpha and CXCL8 via reactive oxygen species and mitogen-activated protein kinase activation. Toxicol Appl Pharmacol 238:160–169.

Lichten LA, Liuzzi JP, Cousins RJ. 2009. Interleukin-1beta contributes via nitric oxide to the upregulation and functional activity of the zinc transporter Zip14 (Slc39a14) in murine hepatocytes. Am J Physiol Gastrointest Liver Physiol 296: G860–867.

Lin CH, Chang LW, Chang H, Yang MH, Yang CS, Lai WH, et al. 2009. The chemical fate of the Cd/Se/Te-based quantum dot 705 in the biological system: Toxicity implications. Nanotechnology 20:215101.

Lin P, Chen JW, Chang WH, Wu JP, Redding L, Chang H, et al. 2008. Computational and structural toxicology of a nanoparticle, quantum dot 705, in mice. Environ Sci Tech 42:6264–6270.

Lores Arnaiz S, Llesuy S, Cutrin JC, Boveris A. 1995. Oxidative stress by acute acetaminophen administration in mouse liver. Free Radic Biol Med 19:303–310.

Lovric J, Cho SJ, Winnik FM, Maysinger D. 2005. Unmodified cadmium telluride quantum dots induce reactive oxygen species formation leading to multiple organelle damage and cell death. Chem Biol 12:1227–1234.

Mahto SK, Park C, Yoon TH, Rhee SW. 2010. Assessment of cytocompatibility of surface-modified CdSe/ZnSe quantum dots for BALB/3T3 fibroblast cells. Toxicol In Vitro 24:1070–1077.

Min KS, Ueda H, Kihara T, Tanaka K. 2008. Increased hepatic accumulation of ingested Cd is associated with upregulation of several intestinal transporters in mice fed diets deficient in essential metals. Toxicol Sci 106:284–289.

Monteiro-Riviere NA, Inman AO, Zhang LW. 2009. Limitations and relative utility of screening assays to assess engineered nanoparticle toxicity in a human cell line. Toxicol Appl Pharmacol 234:222–235.

Moreno MG, Muriel P. 2006. Inducible nitric oxide synthase is not essential for the development of fibrosis and liver damage induced by CCl4 in mice. J Appl Toxicol 26:326–332.

Mulder WJ, Strijkers GJ, Nicolay K, Griffioen AW. 2010. Quantum dots for multimodal molecular imaging of angiogenesis. Angiogenesis 13:131–134.

Nel A, Xia T, Madler L, Li N. 2006. Toxic potential of materials at the nanolevel. Science 311:622–627.

Obonyo O, Fisher E, Edwards M, Douroumis D. 2010. Quantum dots synthesis and biological applications as imaging and drug delivery systems. Crit Rev Biotechnol: 1–19.

Ravanat JL, Douki T, Duez P, Gremaud E, Herbert K, Hofer T, et al. 2002. Cellular background level of 8-oxo-7,8-dihydro-2′-deoxyguanosine: An isotope based method to evaluate artefactual oxidation of DNA during its extraction and subsequent work-up. Carcinogenesis 23:1911–1918.

Samia AC, Chen X, Burda C. 2003. Semiconductor quantum dots for photodynamic therapy. J Am Chem Soc 125:15736–15737.

Shiohara A, Hoshino A, Hanaki K, Suzuki K, Yamamoto K. 2004. On the cyto-toxicity caused by quantum dots. Microbiol Immunol 48:669–675.

Sies H. 1993. Strategies of antioxidant defense. Eur J Biochem 215:213–219.

Singh N, Manshian B, Jenkins GJ, Griffiths SM, Williams PM, Maffeis TG, et al. 2009. NanoGenotoxicology: The DNA damaging potential of engineered nanomaterials. Biomaterials 30:3891–3914.

Smith AM, Duan H, Mohs AM, Nie S. 2008. Bioconjugated quantum dots for in vivo molecular and cellular imaging. Adv Drug Deliv Rev 60:1226–1240.

Song IS, Chen HH, Aiba I, Hossain A, Liang ZD, Klomp LW, et al. 2008. Transcription factor Sp1 plays an important role in the regulation of copper homeostasis in mammalian cells. Mol Pharmacol 74:705–713.

Wu Y, Li X, Steel D, Gammom D, Sham LJ. 2004. Coherent optical control of semiconductor quantum dots for quantum information processing. Physica E: Low-Dimens Syst Nanostruct 25:242–248.

Yang RS, Chang LW, Wu JP, Tsai MH, Wang HJ, Kuo YC, et al. 2007. Persistent tissue kinetics and redistribution of nanoparticles, quantum dot 705, in mice: ICP-MS quantitative assessment. Environ Health Perspect 115:1339–1343.

Youn CK, Kim SH, Lee DY, Song SH, Chang IY, Hyun JW, et al. 2005. Cadmium down-regulates human OGG1 through suppression of Sp1 activity. J Biol Chem 280:25185–25195.

Zhang LW, Yu WW, Colvin VL, Monteiro-Riviere NA. 2008. Biological interactions of quantum dot nanoparticles in skin and in human epidermal keratinocytes. Toxicol Appl Pharmacol 228:200–211.

Zharkov DO, Rosenquist TA. 2002. Inactivation of mammalian 8-oxoguanine-DNA glycosylase by cadmium(II): Implications for cadmium genotoxicity. DNA Repair (Amst) 1: 661–670.